Available online at www.sciencedirect.com
SCIENCE DIRECT®
Computers & Fluids 34 (2005) 561–580
computers & fluids
www.elsevier.com/locate/compfluid

A residual-based compact scheme for the unsteady compressible Navier–Stokes equations

C. Corre, G. Hanss, A. Lerat *

SINUMEF Laboratory, ENSAM, 151 Boulevard de l'Hôpital, Paris 75013, France

Received 3 April 2003; accepted 27 August 2003
Available online 6 May 2004

Abstract

A dissipative compact scheme is developed within a dual time stepping framework for the computation of unsteady compressible flows. The design of the scheme relies on the vanishing, at steady state with respect to the dual time, of a residual that includes the physical time-derivative. High-order accuracy and numerical dissipation are obtained in a simple way through the systematic use of derivatives of this residual. The accuracy and robustness of the approach are assessed on the simple advection of an inviscid vortex and compressible mixing layer problems involving shock waves.

1. Introduction

In Computational Fluid Dynamics, high accurate schemes based on compact stencils ([1–11] for instance) have several advantages over their non-compact analogues. For the same order of accuracy, a narrower stencil usually reduces the truncation error constant, makes easier the extension to distorted meshes, simplifies the boundary condition treatment and increases the efficiency of an implicit formulation of the scheme. In a classical compact scheme, a derivative in a coordinate direction is approximated from a reduced number of points in this direction, for instance by using a Pade formula. Here, we consider a compact approximation that provides a high order of accuracy not for each space derivative treated apart but only for the whole residual r (all the terms of the equation to be solved). This non-directional approach is said to be *residual-based compact* (RBC). We thus continue the investigation of RBC schemes begun in [12] for the steady

* Corresponding author. Tel.: +33-1-4424-6248; fax: +33-1-4424-6275.
E-mail address: alain.lerat@paris.ensam.fr (A. Lerat).

0045-7930/$ - see front matter
doi:10.1016/j.compfluid.2003.08.003

Euler equations and in [13] for the steady Navier–Stokes equations. The aim of the present paper is to extend the method to *unsteady* compressible flows. For steady problems, r is the residual at steady state. For unsteady problems, r will include the time derivative but it will be still considered as a steady-state residual with respect to a dual time.

Dealing with the residual is also favourable for constructing the numerical dissipation necessary for compressible flow computations including shock waves. A residual-based dissipation contains derivatives of the residual only and thus is consistent with a partial differential operator vanishing at steady state. Such a dissipation can be of first order in the transient phase and therefore can provide robustness in a simple way, without degrading the high accuracy at steady state (in real or dual time) and the compactness.

The paper is organized as follows. Section 2 reviews the way of getting high-order accuracy in space for inviscid and viscous problems on structured grids using residual-based compactness and a residual-based numerical dissipation operator. Section 3 presents a residual-based scheme for computing unsteady solutions of the compressible Euler and Navier–Stokes equations within a dual time framework. Finally, numerical experiments are presented in Section 4. The first test case is an inviscid problem, the advection of an inviscid vortex, the well-known exact solution of which allows to assess the accuracy properties of the proposed scheme; the second and third test case are compressible mixing layer computations taken from [14]. These DNS type problems were selected in order to focus on the scheme properties for the computation of complex compressible viscous flows without any incidence of turbulence modelling.

2. Residual-based scheme for computing steady compressible flows

2.1. Fourth-order approximation

Consider the spatial approximation of the two-dimensional Euler equations:

$$w_t + f^{\mathrm{E}}(w)_x + g^{\mathrm{E}}(w)_y = 0 \tag{1}$$

where t is the time, x and y are space coordinates, $w = w(x, y, t)$ is the state vector, f^{E} and g^{E} are flux vector functions depending smoothly on w. Let $v_{j,k}$ be a mesh function defined on a uniform Cartesian mesh ($x_j = j\delta x, y_k = k\delta y$), with steps δx and δy of the same order, say $\mathrm{O}(h)$. Let us define the basic difference and average operators:

$$(\delta_1 v)_{j+\frac{1}{2},k} = v_{j+1,k} - v_{j,k}, \quad (\delta_2 v)_{j,k+\frac{1}{2}} = v_{j,k+1} - v_{j,k}$$

$$(\mu_1 v)_{j+\frac{1}{2},k} = \frac{1}{2}(v_{j+1,k} + v_{j,k}), \quad (\mu_2 v)_{j,k+\frac{1}{2}} = \frac{1}{2}(v_{j,k+1} + v_{j,k})$$

The classical non-compact fourth-order approximation for the space derivatives f^{E}_x and g^{E}_y reads:

$$\frac{1}{\delta x}\delta_1\mu_1\left(I - \frac{1}{6}\delta_1^2\right)f^{\mathrm{E}} = f^{\mathrm{E}}_x + \mathrm{O}(h^4)$$

$$\frac{1}{\delta y}\delta_2\mu_2\left(I - \frac{1}{6}\delta_2^2\right)g^{\mathrm{E}} = g^{\mathrm{E}}_y + \mathrm{O}(h^4)$$

where I is the identity operator and the subscripts j,k are omitted for concision. This approximation involves five points per direction. Alternatively, a compact fourth-order approximation can be written with Pade fractions (using three points per direction only) but the price to pay for this compact stencil is the numerical solution of a linear algebraic system for each space direction. However it is possible to avoid this extra cost when calculating steady solutions. The idea is no longer to correct the truncation error on each space derivative, but to consider the whole residual at steady state $r = f_x^{\mathrm{E}} + g_y^{\mathrm{E}}$ and to devise a scheme based on a 3×3-point stencil with a global truncation error that can be expressed in terms of derivatives of r only. More precisely, let us consider the scheme:

$$w_t + \frac{1}{\delta x}\delta_1\mu_1\left(I + \frac{1}{6}\delta_2^2\right)f^{\mathrm{E}} + \frac{1}{\delta y}\delta_2\mu_2\left(I + \frac{1}{6}\delta_1^2\right)g^{\mathrm{E}} = 0 \tag{2}$$

Its truncation error is given by

$$\begin{aligned}\epsilon &= w_t + r + \frac{\delta x^2}{6}\left(f_{xxx}^{\mathrm{E}} + g_{xxy}^{\mathrm{E}}\right) + \frac{\delta y^2}{6}\left(f_{xyy}^{\mathrm{E}} + g_{yyy}^{\mathrm{E}}\right) + \mathrm{O}(h^4)\\ &= w_t + r + \frac{\delta x^2}{6}r_{xx} + \frac{\delta y^2}{6}r_{yy} + \mathrm{O}(h^4)\end{aligned}$$

so that for an exact steady solution, $w_t = r = 0$ and $\epsilon = \mathrm{O}(h^4)$, yielding fourth-order accuracy at steady state without requiring any linear algebra. This type of approximation will be called *residual-based compactness*.

2.2. Numerical dissipation

To be able to run the above method for compressible flows, some numerical dissipation is required. The present dissipation is also residual-based, i.e. constructed from derivatives of the residual r. This is advantageous because such a dissipation can be of order h in the transient phase and therefore can provide robustness in a simple way, while preserving a high accuracy at steady state. Consider the compact scheme (2); on the right-hand side of (2), a centered discretization of the following operator is added:

$$P = \frac{\delta x}{2}(\Phi_1 r)_x + \frac{\delta y}{2}(\Phi_2 r)_y \tag{3}$$

where Φ_1 and Φ_2 are matricial coefficients depending only on the space increments δx, δy and on the flux Jacobian matrices $A^{\mathrm{E}} = \mathrm{d}f^{\mathrm{E}}/\mathrm{d}w$, $B^{\mathrm{E}} = \mathrm{d}g^{\mathrm{E}}/\mathrm{d}w$: $\Phi_1 = \Phi_1(A^{\mathrm{E}}, B^{\mathrm{E}}; \delta x, \delta y) = \mathrm{O}(1)$, $\Phi_2 = \Phi_2(A^{\mathrm{E}}, B^{\mathrm{E}}; \delta x, \delta y) = \mathrm{O}(1)$. The operator P is independent of Δt and therefore the same holds for the computed steady solution.

First, let us check that the above first-order dissipation is compatible with a high accuracy. Adding to the right-hand side of scheme (2) a (second-order) centered discretization $\widetilde{P}$ of the operator P yields a dissipative scheme with truncation error:

$$\epsilon = w_t + r + \frac{\delta x^2}{6}r_{xx} + \frac{\delta y^2}{6}r_{yy} + \mathrm{O}(h^4) - \frac{\delta x}{2}(\Phi_1 r)_x - \frac{\delta y}{2}(\Phi_2 r)_y + \mathrm{O}(h^3)$$

so that for an exact steady solution $\epsilon = \mathrm{O}(h^3)$. During the transient phase, the dissipative scheme is first-order accurate, but it becomes third-order accurate at steady state. Dissipation at steady

state is provided by the truncation error in the approximation of P. In [13], it has been checked that the solution error converges very quickly to third order during the evolution to steady state.

Functions Φ_1 and Φ_2 are chosen so that the operator P be dissipative, i.e. bring parabolicity. It was proved (see [13]) in the scalar case that the following choice:

$$\Phi_1 = \mathrm{sgn}(A^{\mathrm{E}}) \min\left(1, \frac{1}{\alpha}\right), \quad \Phi_2 = \mathrm{sgn}(B^{\mathrm{E}}) \min(1, \alpha), \quad \alpha = \frac{\delta x |B^{\mathrm{E}}|}{\delta y |A^{\mathrm{E}}|}$$

allows to minimize the numerical dissipation associated with $\widetilde{P}$. Note that Φ_1 and Φ_2 have nothing to do with limiters: their expression does not involve any slopes, gradients or shock sensors and is uniquely defined by the previously stated requirement that they should ensure the scheme dissipation. For the Euler equations, the matricial functions Φ_1 and Φ_2 are defined through a straightforward extension of this scalar case: the eigenvectors of Φ_1 (respectively Φ_2) are those of A^{E} (resp. B^{E}) and the eigenvalues are deduced from the above scalar definitions of Φ_1 (resp. Φ_2). If $T_{A^{\mathrm{E}}}$ (resp. $T_{B^{\mathrm{E}}}$) is a matrix whose column vectors are the right eigenvectors of the Jacobian matrix A^{E} (resp. B^{E}) and if $(a^{\mathrm{E}})^{(i)}$ (resp. $(b^{\mathrm{E}})^{(i)}$) denote the eigenvalues of A^{E} (resp. B^{E}) then the matrices Φ_1 and Φ_2 are defined by

$$\Phi_1 = T_{A^{\mathrm{E}}} \mathrm{Diag}[\phi_1^{(i)}] T_{A^{\mathrm{E}}}^{-1}, \quad \Phi_2 = T_{B^{\mathrm{E}}} \mathrm{Diag}[\phi_2^{(i)}] T_{B^{\mathrm{E}}}^{-1} \tag{4}$$

with

$$\phi_1^{(i)} = \mathrm{sgn}((a^{\mathrm{E}})^{(i)}) \phi^{(i)}, \quad \phi_2^{(i)} = \mathrm{sgn}((b^{\mathrm{E}})^{(i)}) \psi^{(i)} \tag{5}$$

$$\phi^{(i)} = \min\left(1, \frac{\delta y |(a^{\mathrm{E}})^{(i)}|}{\delta x\, m(B^{\mathrm{E}})}\right), \quad \psi^{(i)} = \min\left(1, \frac{\delta x |(b^{\mathrm{E}})^{(i)}|}{\delta y\, m(A^{\mathrm{E}})}\right) \tag{6}$$

where $\mathrm{Diag}[d^{(i)}]$ denotes a diagonal matrix with diagonal entries $d^{(i)}$ and $m(A^{\mathrm{E}}) = \min_i(|(a^{\mathrm{E}})^{(i)}|)$, $m(B^{\mathrm{E}}) = \min_i(|(b^{\mathrm{E}})^{(i)}|)$.

2.3. Fully discrete scheme for the Euler equations

Let us come to the full description of scheme (2) with dissipation. When we are only interested in steady solutions, the time-derivative in (2) may be simply approximated using an Euler forward difference. Now, to ensure linear stability and dissipation for the fully discrete scheme, it is important to discretize P properly. Similarly as in [17,18] for the Lax–Wendroff method, we compute the residuals for numerical dissipation at cell interfaces $j+\frac{1}{2}, k$ and $j, k+\frac{1}{2}$. The explicit version of the scheme reads:

(a) Residuals for numerical dissipation:

$$\begin{aligned} (\Pi_1)^n_{j+\frac{1}{2},k} &= \left(\frac{\delta_1 f^{\mathrm{E}}}{\delta x} + \frac{\delta_2 \mu_1 \mu_2 g^{\mathrm{E}}}{\delta y}\right)^n_{j+\frac{1}{2},k} \\ (\Pi_2)^n_{j,k+\frac{1}{2}} &= \left(\frac{\delta_1 \mu_1 \mu_2 f^{\mathrm{E}}}{\delta x} + \frac{\delta_2 g^{\mathrm{E}}}{\delta y}\right)^n_{j,k+\frac{1}{2}} \end{aligned} \tag{7}$$

(b) Numerical fluxes:

$$(h_1)^n_{j+\frac{1}{2},k} = \left[\left(I + \frac{1}{6}\delta_2^2\right)\mu_1 f^{\mathrm{E}} - \frac{\delta x}{2}\Phi_1 \Pi_1\right]^n_{j+\frac{1}{2},k}$$
$$(h_2)^n_{j,k+\frac{1}{2}} = \left[\left(I + \frac{1}{6}\delta_1^2\right)\mu_2 g^{\mathrm{E}} - \frac{\delta y}{2}\Phi_2 \Pi_2\right]^n_{j,k+\frac{1}{2}} \tag{8}$$

(c) Explicit increment:

$$\Delta w^{\mathrm{expl}}_{j,k} = -\Delta t\left(\frac{\delta_1 F}{\delta x} + \frac{\delta_2 G}{\delta y}\right)^n_{j,k}$$
$$w^{n+1}_{j,k} = w^n_{j,k} + \Delta w^{\mathrm{expl}}_{j,k} \tag{9}$$

In these expressions, $w^n_{j,k}$ denotes the numerical solution at time level $n\Delta t$ and location $(j\delta x, k\delta y)$, the matrices Φ_1 and Φ_2 are computed from (4)–(6) using Roe averages A^{E}_R and B^{E}_R to define A^{E} and B^{E} at cell interfaces $j+\frac{1}{2},k$ and $j,k+\frac{1}{2}$. The 3×3 point explicit scheme (7)–(9) is third-order accurate at steady state. It is rather simple and requires no limiters or other corrections.

2.4. Fully discrete scheme for the Navier–Stokes equations

The Navier–Stokes equations can be written in the following form:

$$w_t + \left(f^{\mathrm{E}} - f^{\mathrm{V}}\right)_x + \left(g^{\mathrm{E}} - g^{\mathrm{V}}\right)_y = 0 \tag{10}$$

where f^{E} and g^{E} still denote the Euler fluxes and $f^{\mathrm{V}} = f^{\mathrm{V}}(w, w_x, w_y)$, $g^{\mathrm{V}} = g^{\mathrm{V}}(w, w_x, w_y)$ stand for the viscous fluxes. System (10) is discretized in the same way as system (1), that is

$$\frac{w^{n+1} - w^n}{\Delta t} + \tilde{r}^n = \tilde{P}^n \tag{11}$$

where $\tilde{r}^n$ denotes a centered approximation to the steady-state residual $r = \left(f^{\mathrm{E}} - f^{\mathrm{V}}\right)_x + \left(g^{\mathrm{E}} - g^{\mathrm{V}}\right)_y$ and $\tilde{P}^n$ is a centered approximation to (3) in which only the definition of r has changed to include now inviscid and viscous fluxes. Note that since the operator P now contains third-order derivatives, it is no longer purely dissipative. To simplify the presentation of the fully discrete scheme, we assume that the viscous fluxes read:

$$f^{\mathrm{V}} = \nu^{(1)} w_x + \nu^{(2)} w_y, \quad g^{\mathrm{V}} = \nu^{(3)} w_x + \nu^{(4)} w_y \tag{12}$$

where $\nu^{(1)}$, $\nu^{(2)}$, $\nu^{(3)}$ and $\nu^{(4)}$ are constant viscosity coefficients ensuring physical dissipation, i.e. such that $\nu^{(1)} \geqslant 0$, $\nu^{(4)} \geqslant 0$ and $\left(\nu^{(2)} + \nu^{(3)}\right)^2 \leqslant 2\nu^{(1)}\nu^{(4)}$. We also introduce the following notations for the discrete viscous fluxes:

$$\left(\tilde{f}^{\mathrm{V}}(w_x, w_y)\right)_{j+\frac{1}{2},k} = \left(\tilde{f}^{\mathrm{V}}_n(w_x) + \tilde{f}^{\mathrm{V}}_t(w_y)\right)_{j+\frac{1}{2},k} = \left(\nu^{(1)}\frac{\delta_1 w}{\delta x} + \nu^{(2)}\frac{\delta_2 \mu_1 \mu_2 w}{\delta y}\right)_{j+\frac{1}{2},k}$$

$$\left(\tilde{\tilde{g}}^{\mathrm{V}}(w_x, w_y)\right)_{j,k+\frac{1}{2}} = \left(\tilde{\tilde{g}}^{\mathrm{V}}_t(w_x) + \tilde{\tilde{g}}^{\mathrm{V}}_n(w_y)\right)_{j,k+\frac{1}{2}} = \left(\nu^{(3)}\frac{\delta_1 \mu_1 \mu_2 w}{\delta x} + \nu^{(4)}\frac{\delta_2 w}{\delta y}\right)_{j,k+\frac{1}{2}}$$

The predictors and numerical fluxes of the fully discrete scheme then read:

(a) Predictors:

$$(\Pi_1)^n_{j+\frac{1}{2},k} = \left[\frac{\delta_1(f^{\mathrm{E}} - \mu_1\tilde{f}^{\mathrm{V}})}{\delta x} + \frac{\delta_2(\mu_1\mu_2 g^{\mathrm{E}} - \mu_1\tilde{\tilde{g}}^{\mathrm{V}})}{\delta y}\right]^n_{j+\frac{1}{2},k}$$
$$(\Pi_2)^n_{j,k+\frac{1}{2}} = \left[\frac{\delta_1(\mu_1\mu_2 f^{\mathrm{E}} - \mu_2\tilde{f}^{\mathrm{V}})}{\delta x} + \frac{\delta_2(g^{\mathrm{E}} - \mu_2\tilde{\tilde{g}}^{\mathrm{V}})}{\delta y}\right]^n_{j,k+\frac{1}{2}} \tag{13}$$

(b) Numerical fluxes:

$$(h_1)^n_{j+\frac{1}{2},k} = \left[\left(I + \frac{1}{6}\delta_2^2\right)(\mu_1 f^{\mathrm{E}} - \tilde{f}^{\mathrm{V}}_n) - \tilde{f}^{\mathrm{V}}_t - \frac{1}{12}\delta_1^2\tilde{f}^{\mathrm{V}}_n - \frac{\delta x}{2}\Phi_1\Pi_1\right]^n_{j+\frac{1}{2},k}$$
$$(h_2)^n_{j,k+\frac{1}{2}} = \left[\left(I + \frac{1}{6}\delta_1^2\right)(\mu_2 g^{\mathrm{E}} - \tilde{\tilde{g}}^{\mathrm{V}}_n) - \tilde{\tilde{g}}^{\mathrm{V}}_t - \frac{1}{12}\delta_2^2\tilde{\tilde{g}}^{\mathrm{V}}_n - \frac{\delta y}{2}\Phi_2\Pi_2\right]^n_{j,k+\frac{1}{2}} \tag{14}$$

(c) Explicit increment:

$$\Delta w^n_{j,k} = w^{n+1}_{j,k} - w^n_{j,k} = -\Delta t\left(\frac{\delta_1 h_1}{\delta x} + \frac{\delta_2 h_2}{\delta y}\right)^n_{j,k} \tag{15}$$

It is easy to check (see [13] for details) that the above numerical fluxes yield $\tilde{r} = r + \frac{\delta x^2}{6}r_{xx} + \frac{\delta y^2}{6}r_{yy} + \mathrm{O}(h^4)$ and $\tilde{P} = P + \mathrm{O}(h^3)$; scheme (13)–(15) is therefore a third-order accurate approximation of (10) at steady state. Note that for viscous flow problems, the functions Φ_1 and Φ_2 could take into account the physical viscosity in order to reduce the numerical dissipation in viscous layers. In the present work however, we retain for viscous applications the functions Φ_1, Φ_2 defined by (4)–(6) for the Euler equations: this choice has no incidence on the order of accuracy.

3. A residual-based scheme for unsteady compressible flows

3.1. Inviscid case

We are now looking for a time and space-accurate approximation of the 2D Euler equations (1). An approximate solution of (1) can be efficiently obtained using an implicit linear multi-step method of the form:

$$T(w^{n+1}, w^n, w^{n-1}) + R(w^{n+1}) = 0 \tag{16}$$

where R denotes a space-discretization operator that will be detailed later and T is a three-step approximation of w_t at time-level $(n+1)$ defined by

$$T(w^{n+1}, w^n, w^{n-1}) = (1+\phi)\frac{\Delta w^n}{\Delta t} - \phi\frac{\Delta w^{n-1}}{\Delta t} = (w_t)^{n+1} + \mathrm{O}(\Delta t^p) \tag{17}$$

With $\phi = 0$, (17) yields a simple first-order Euler discretization while $\phi = 1/2$ allows to reach second-order accuracy in time through the use of a third time-level $(n-1)$. In order to efficiently solve the implicit system $R^*(w^{n+1}) = 0$, where $R^*(w^{n+1}) = T(w^{n+1}, w^n, w^{n-1}) + R(w^{n+1})$, one makes use of a dual time technique, well known for incompressible flow calculations [15] and made popular by Jameson [16] for computing compressible flows. This means w^{n+1} is obtained as the steady solution of an evolution problem with respect to a dual or fictitious time τ:

$$w_\tau + R^*(w) = 0.$$

More precisely, starting from the initial guess $w^{n,0} = w^n$, we look for the steady solution of

$$\frac{\Delta w^{n,m}}{\Delta \tau} + T(w^{n,m}, w^n, w^{n-1}) + R(w^{n,m}) = 0 \tag{18}$$

where $\Delta w^{n,m} = w^{n,m+1} - w^{n,m}$. For this approach to be efficient, it is naturally desirable to obtain a good approximation of the steady solution after a small number of subiterations m; this is achieved through the implicitation of relation (18) with respect to the dual time:

$$\frac{\Delta w^{n,m}}{\Delta \tau} + T(w^{n,m+1}, w^n, w^{n-1}) + R(w^{n,m+1}) = 0$$

Introducing the parameter $\lambda = (1+\phi)\frac{\Delta\tau}{\Delta t}$ and denoting R_i the part of the space discretization operator that is actually made linearly implicit, the scheme solved at each subiteration takes the form:

$$(I + \lambda I + R_i)\Delta w^{n,m} = -\Delta\tau R(w^{n,m}) - \Delta\tau T(w^{n,m}, w^n, w^{n-1}) \tag{19}$$

where the term $\lambda \Delta w^{n,m}$ comes from the implicitation of the physical time-derivative approximation.

A second order in time and space simply centered scheme corresponds to $\phi = \frac{1}{2}$ and $R(w) = \frac{\delta_1\mu_1 f^{\mathrm{E}}}{\delta x} + \frac{\delta_2\mu_2 g^{\mathrm{E}}}{\delta y}$ in (16). The truncation error associated with this scheme reads:

$$\epsilon = (w_t)^{n+1} - \frac{1}{3}\Delta t^2 (w_{3t})^{n+1} + \mathrm{O}(\Delta t^3) + (f_x)^{n+1} + \frac{1}{6}\delta x^2 (f_{3x})^{n+1} + (g_y)^{n+1} + \frac{1}{6}\delta y^2 (g_{3y})^{n+1} + \mathrm{O}(\delta x^4, \delta y^4)$$

To reach third-order accuracy in space, we add second-order terms to the above scheme so as to express the truncation error in terms of the residual $r = w_t + f_x^{\mathrm{E}} + g_y^{\mathrm{E}}$ and its derivatives only. More precisely, we approximate r by the following discrete expression:

$$\tilde{r}^{n+1} = \left(I + \frac{\delta_1^2}{6}\right)\left(I + \frac{\delta_2^2}{6}\right) T(w^{n+1}, w^n, w^{n-1}) + \left(I + \frac{\delta_2^2}{6}\right)\frac{\delta_1\mu_1}{\delta x}(f^{\mathrm{E}})^{n+1} + \left(I + \frac{\delta_1^2}{6}\right)\frac{\delta_2\mu_2}{\delta y}(g^{\mathrm{E}})^{n+1} \tag{20}$$

and it is then easy to check that:

$$\tilde{r}^{n+1} = r^{n+1} + \frac{\delta x^2}{6} r_{xx}^{n+1} + \frac{\delta y^2}{6} r_{yy}^{n+1} - \frac{\Delta t^2}{3} w_{3t}^{n+1} + \mathrm{O}(\Delta t^3, h^4, \Delta t^2 h^2)$$

which means $\tilde{r}^{n+1}$ approximates (1) at second order in time and third order in space since $r \equiv 0$ at steady state with respect to the dual time. Note that approximation (20) for r is actually the fourth order in space Pade approximation:

$$T(w^{n+1}, w^n, w^{n-1}) + \frac{1}{\delta x}\frac{\delta_1\mu_1}{I+\frac{\delta_1^2}{6}}f^{\mathrm{E}} + \frac{1}{\delta y}\frac{\delta_2\mu_2}{I+\frac{\delta_2^2}{6}}g^{\mathrm{E}} = 0$$

to which the operator $(I+\frac{\delta_1^2}{6})(I+\frac{\delta_2^2}{6})$ has been applied. Naturally this scheme must be completed with a dissipation-like operator $\tilde{P}$, which is built using the same design principles than in the steady case: $\tilde{P}$ is a centered approximation to the differential operator P given by (3) but with r including now the physical time-derivative. This leads to the following expression:

$$\tilde{P}^{n+1} = \frac{1}{2}\left\{\delta_1\left[\Phi_1\left(\frac{\delta_1 f^{\mathrm{E}}}{\delta x}\right)^{n+1} + \left(\frac{\delta_2\mu_1\mu_2 g^{\mathrm{E}}}{\delta y}\right)^{n+1} + \mu_1 T(w^{n+1}, w^n, w^{n-1})\right]\right.$$
$$\left. + \delta_2\left[\Phi_2\left(\frac{\delta_2\mu_1\mu_2 f^{\mathrm{E}}}{\delta x}\right)^{n+1} + \left(\frac{\delta_2 g^{\mathrm{E}}}{\delta y}\right)^{n+1} + \mu_2 T(w^{n+1}, w^n, w^{n-1})\right]\right\}$$

and $\tilde{P} = P + \mathrm{O}(h^3, h\Delta t^2)$ if the second-order formula (17) with $\phi = 1/2$ is used to approximate the physical time-derivatives. Putting together $\tilde{r}$ and $\tilde{P}$ within the dual time framework, we obtain the scheme $\frac{\Delta w^{n,m}}{\Delta\tau} + \tilde{r}^{n,m} = \tilde{P}^{n,m}$ or in developed form:

RBC scheme for the unsteady Euler equations

(a) Predictors:

$$(\Pi_1)^n_{j+\frac{1}{2},k} = \left[\mu_1 T(w^{n,m}, w^n, w^{n-1}) + \left(\frac{\delta_1 f^{\mathrm{E}}}{\delta x} + \frac{\delta_2\mu_1\mu_2 g^{\mathrm{E}}}{\delta y}\right)^{n,m}\right]_{j+\frac{1}{2},k}$$
$$(\Pi_2)^n_{j,k+\frac{1}{2}} = \left[\mu_2 T(w^{n,m}, w^n, w^{n-1}) + \left(\frac{\delta_1\mu_1\mu_2 f^{\mathrm{E}}}{\delta x} + \frac{\delta_2 g^{\mathrm{E}}}{\delta y}\right)^{n,m}\right]_{j,k+\frac{1}{2}} \tag{21}$$

(b) Numerical fluxes:

$$(h_1)^{n,m}_{j+\frac{1}{2},k} = \left[\left(I+\frac{1}{6}\delta_2^2\right)\mu_1 f^{\mathrm{E}} - \frac{\delta x}{2}\Phi_1\Pi_1\right]^{n,m}_{j+\frac{1}{2},k}$$
$$(h_2)^{n,m}_{j,k+\frac{1}{2}} = \left[\left(I+\frac{1}{6}\delta_1^2\right)\mu_2 g^{\mathrm{E}} - \frac{\delta y}{2}\Phi_2\Pi_2\right]^{n,m}_{j,k+\frac{1}{2}} \tag{22}$$

(c) Explicit increment:

$$\Delta w^{n,m}_{j,k} = -\Delta\tau\left(\frac{\delta_1 h_1}{\delta x} + \frac{\delta_2 h_2}{\delta y}\right)^{n,m}_{j,k} - \left(I+\frac{\delta_1^2}{6}\right)\left(I+\frac{\delta_2^2}{6}\right)\Delta\tau T(w^{n,m}, w^n, w^{n-1}) \tag{23}$$

At steady state with respect to the dual time τ, the scheme (21)–(23) yields a second order in time and third order in space approximation of the Euler equations. The scheme is made implicit as follows:

$$\Delta w^{n,m}_{j,k} + \lambda \Delta w^{n,m}_{j,k} + \delta_1(\dot{A}^{\mathrm{E}}_R \mu_1 \Delta w^{n,m})_{j,k} - \frac{1}{2}\delta_1(|\dot{A}^{\mathrm{E}}|\delta_1 \Delta w^{n,m})_{j,k} + \delta_2(\dot{B}^{\mathrm{E}}\mu_2 \Delta w^{n,m})_{j,k} - \frac{1}{2}\delta_2(|\dot{B}^{\mathrm{E}}|\delta_2 \Delta w^{n,m})_{j,k} = \Delta w^{\exp}_{j,k} \tag{24}$$

where $\dot{A}^{\mathrm{E}}_R = \frac{\Delta t}{\delta x} A^{\mathrm{E}}_R$ and $\dot{B}^{\mathrm{E}}_R = \frac{\Delta t}{\delta y} B^{\mathrm{E}}_R$. Only the terms corresponding to a Harten–Roe type implicit-stage have been retained in order to keep the method simple and cheap. The linear system associated with (24) is solved using an alternate line relaxation technique that allows to reach a steady state with respect to τ in 10–20 subiterations only (see [19] for more details on this technique).

3.2. Extension to the Navier–Stokes equations

When solving the 2D Navier–Stokes equations (10) with a residual-based scheme, the principles detailed in the previous section remain unchanged but have to be applied with a residual defined as $r = w_t + (f^{\mathrm{E}} - f^{\mathrm{V}})_x + (g^{\mathrm{E}} - g^{\mathrm{V}})_y$. A time and space second-order accurate scheme is simply obtained by including centered discretizations of the viscous fluxes f^{V} and g^{V} in the predictors (21) and in the numerical fluxes (22). Third-order accuracy in space is reached by adding to the numerical fluxes the residual-based corrections detailed in Section 2.4 to cancel the second-order error terms of the viscous fluxes discretizations, which yields the following scheme:

RBC scheme for the unsteady Navier–Stokes equations

(a) Predictors:

$$\begin{aligned}
(\Pi_1)^n_{j+\frac{1}{2},k} &= \left[\mu_1 T(w^{n,m}, w^n, w^{n-1}) + \left(\frac{\delta_1}{\delta x}(f^{\mathrm{E}} - \mu_1 \tilde{f}^{\mathrm{V}}) + \frac{\delta_2}{\delta y}(\mu_1\mu_2 g^{\mathrm{E}} - \mu_1 \tilde{\tilde{g}}^{\mathrm{V}})\right)^{n,m}\right]_{j+\frac{1}{2},k} \\
(\Pi_2)^n_{j,k+\frac{1}{2}} &= \left[\mu_2 T(w^{n,m}, w^n, w^{n-1}) + \left(\frac{\delta_1}{\delta x}(\mu_1\mu_2 f^{\mathrm{E}} - \mu_2 \tilde{f}^{\mathrm{V}}) + \frac{\delta_2}{\delta y}(g^{\mathrm{E}} - \mu_2 \tilde{\tilde{g}}^{\mathrm{V}})\right)^{n,m}\right]_{j,k+\frac{1}{2}}
\end{aligned} \tag{25}$$

(b) Numerical fluxes:

$$\begin{aligned}
(h_1)^{n,m}_{j+\frac{1}{2},k} &= \left[\left(I + \frac{1}{6}\delta_2^2\right)(\mu_1 f^{\mathrm{E}} - \tilde{f}^{\mathrm{V}}_n) - \tilde{f}^{\mathrm{V}}_t - \frac{1}{12}\delta_1^2 \tilde{f}^{\mathrm{V}}_n - \frac{\delta x}{2}\Phi_1 \Pi_1\right]^{n,m}_{j+\frac{1}{2},k} \\
(h_2)^{n,m}_{j,k+\frac{1}{2}} &= \left[\left(I + \frac{1}{6}\delta_1^2\right)(\mu_2 g^{\mathrm{E}} - \tilde{\tilde{g}}^{\mathrm{V}}_n) - \tilde{\tilde{g}}^{\mathrm{V}}_t - \frac{1}{12}\delta_2^2 \tilde{\tilde{g}}^{\mathrm{V}}_n - \frac{\delta y}{2}\Phi_2 \Pi_2\right]^{n,m}_{j,k+\frac{1}{2}}
\end{aligned} \tag{26}$$

(c) Explicit increment:

$$\Delta w^{n,m}_{j,k} = -\Delta\tau\left(\frac{\delta_1 h_1}{\delta x} + \frac{\delta_2 h_2}{\delta y}\right)^{n,m}_{j,k} - \left(I + \frac{\delta_1^2}{6}\right)\left(I + \frac{\delta_2^2}{6}\right)\Delta\tau T(w^{n,m}, w^n, w^{n-1}) \tag{27}$$

Scheme (25)–(27) is made implicit following the lines described in (3.1). The viscous Jacobian matrices $A^{\mathrm{V}}_1 = \frac{\partial f^{\mathrm{V}}}{\partial w_x}$ and $B^{\mathrm{V}}_2 = \frac{\partial g^{\mathrm{V}}}{\partial w_y}$ are introduced to take into account the implicitation of $\tilde{f}^{\mathrm{V}} = \tilde{f}^{\mathrm{V}}_n + \tilde{f}^{\mathrm{V}}_t$ and $\tilde{\tilde{g}}^{\mathrm{V}} = \tilde{\tilde{g}}^{\mathrm{V}}_n + \tilde{\tilde{g}}^{\mathrm{V}}_t$ in (26) and the resulting scheme reads:

$$\Delta w^{n,m}_{j,k} + \lambda \Delta w^{n,m}_{j,k} + \delta_1 (\dot{A}^{\mathrm{E}}_R \mu_1 \Delta w^{n,m})_{j,k} - \frac{1}{2}\delta_1((|\dot{A}^{\mathrm{E}}| + \dot{A}^{\mathrm{V}}_1)\delta_1 \Delta w^{n,m})_{j,k} + \delta_2(\dot{B}^{\mathrm{E}} \mu_2 \Delta w^{n,m})_{j,k} - \frac{1}{2}\delta_2((|\dot{B}^{\mathrm{E}}| + \dot{B}^{\mathrm{V}}_2)\delta_2 \Delta w^{n,m})_{j,k} = \Delta w^{\exp}_{j,k} \tag{28}$$

where $\Delta w^{\exp}$ is given by (27) and $\dot{A}^{\mathrm{V}}_1 = \frac{\Delta t}{\delta x^2} A^{\mathrm{V}}_1$, $\dot{B}^{\mathrm{V}}_2 = \frac{\Delta t}{\delta y^2} B^{\mathrm{V}}_2$.

In the following section, the residual-based scheme will be applied to the computation of some unsteady compressible flow problems. To allow a clear appreciation of the scheme properties, the numerical results it provides will be compared with those given by a conventional high-order scheme here referred to as Directional Non-Compact (DNC). This scheme is an extension to the Navier–Stokes equations of the one proposed in [20] to solve the Euler equations. The second-order error terms of the simply centered discretization of the inviscid fluxes f^{E} and g^{E} are cancelled using third-order differences in each space direction. Third-order matrix dissipation is added in each space direction so that the resulting scheme is similar to the well-known Roe-MUSCL scheme (third-order version without limiter or entropy correction). The viscous fluxes are discretized at second order only using centered differences so that the fully discrete schemes eventually reads:

DNC scheme for the unsteady Navier–Stokes equations

(a) Numerical fluxes:

$$\begin{aligned}(h_1)^{n,m}_{j+\frac{1}{2},k} &= \left[\left(I - \frac{1}{6}\delta_1^2\right)\mu_1 f^{\mathrm{E}} - \tilde{f}^{\mathrm{V}} + \frac{1}{12}|A^{\mathrm{E}}_R|\delta_1^3 w\right]^{n,m}_{j+\frac{1}{2},k} \\ (h_2)^{n,m}_{j,k+\frac{1}{2}} &= \left[\left(I - \frac{1}{6}\delta_2^2\right)\mu_2 g^{\mathrm{E}} - \tilde{\tilde{g}}^{\mathrm{V}} + \frac{1}{12}|B^{\mathrm{E}}_R|\delta_2^3 w\right]^{n,m}_{j,k+\frac{1}{2}}\end{aligned} \tag{29}$$

(b) Explicit increment:

$$\Delta w^{n,m}_{j,k} = -\Delta\tau\left(\frac{\delta_1 h_1}{\delta x} + \frac{\delta_2 h_2}{\delta y}\right)^{n,m}_{j,k} - \Delta\tau T(w^{n,m}, w^n, w^{n-1}) \tag{30}$$

Scheme (29) and (30) is used with a second-order approximation ($\phi = 1/2$) for the physical time-derivative. Its implicit stage is identical to that of the residual-based scheme.

4. Applications

Three test-cases are considered in order to assess the properties of the proposed RBC scheme when computing unsteady flows. The first test-case is the advection of a vortex, the second test-case is the vortex pairing in a time-developing mixing layer while the last problem is the impingement of a shock wave on a spatially evolving mixing layer. These problems are inspired or taken from the work by Yee et al. [14].

4.1. Advection of an inviscid vortex

A vortex is added to a uniform freestream flow. The freestream density and pressure are given by $\rho_\infty = 1$, $p_\infty = 1/\gamma$ with $\gamma = 1.4$ the ratio of specific heats. The freestream flow velocity components are chosen such that $u_\infty = v_\infty = \sqrt{2}$ in order to yield an advection at supersonic speed along the grid diagonal. The problem is therefore fully multi-dimensional. The vortex is chosen isentropic with no perturbation in entropy. The perturbation values are those given in [14]:

$$(\delta u, \delta v) = \frac{\Gamma}{2\pi} \mathrm{e}^{\frac{1-r^2}{2}} (-\bar{y}, \bar{x})$$

$$\delta T = -\frac{(\gamma - 1)\Gamma^2}{8\gamma\pi^2} \mathrm{e}^{1-r^2}$$

where Γ denotes the vortex strength equal to 5, $T = p/\rho$, $\bar{x} = x - x_{c_0}$ and $\bar{y} = y - y_{c_0}$ with (x_{c_0}, y_{c_0}) the initial coordinates of the vortex and $r = \sqrt{\bar{x}^2 + \bar{y}^2}$. The initial primitive variables are then build from $u = u_\infty + \delta u$, $v = v_\infty + \delta v$, $T = T_\infty + \delta T$ and the relation $\frac{p}{\rho^\gamma} = \frac{p_\infty}{\rho_\infty^\gamma} = S_\infty$:

$$\begin{aligned}
\rho^0 &= \left[\frac{1}{S_\infty} \left(T_\infty - \frac{(\gamma - 1)\Gamma^2}{8\gamma\pi^2} \mathrm{e}^{1-r^2} \right) \right]^{\frac{1}{\gamma - 1}} \\
u^0 &= u_\infty - \frac{\Gamma}{2\pi} \mathrm{e}^{\frac{1-r^2}{2}} \bar{y} \\
v^0 &= v_\infty + \frac{\Gamma}{2\pi} \mathrm{e}^{\frac{1-r^2}{2}} \bar{x} \\
p^0 &= S_\infty (\rho^0)^\gamma
\end{aligned} \tag{31}$$

The initial state w^0 for the conservative variables follows immediately. The exact solution of the Euler equations (1) with this given initial state is $w(t, x, y) = w_0(\bar{x}, \bar{y})$ with $\bar{x} = x - (x_{c_0} + u_\infty t)$, $\bar{y} = y - (y_{c_0} + v_\infty t)$. The vortex should therefore be passively advected by the supersonic freestream. Numerically, one expects to observe of course the occurrence of dissipative and dispersive errors that can be directly quantified. The computational domain extends from -15 to $+15$ in the x and y direction and the center of the vortex is initially located at $(x_{c_0} = -10, y_{c_0} = -10)$. This domain is uniformly discretized in the x and y directions using 100 points in each direction. A time-step $\Delta t = 0.025$ is used to compute the vortex evolution up to $t = 14$, at which time the vortex center of the exact solution is located close to $x = 9.799, y = 9.799$. The results obtained using RBC and DNC are plotted on Figs. 1 and 2. Fig. 1 allows to observe the reduced dispersive error provided by the residual-based approach over a conventional scheme as well as the limited dissipative error of the RBC scheme. The same comments hold for Fig. 2 where cutlines of density are plotted at the final time of computation along horizontal and vertical lines passing through the theoretical location of the vortex center.

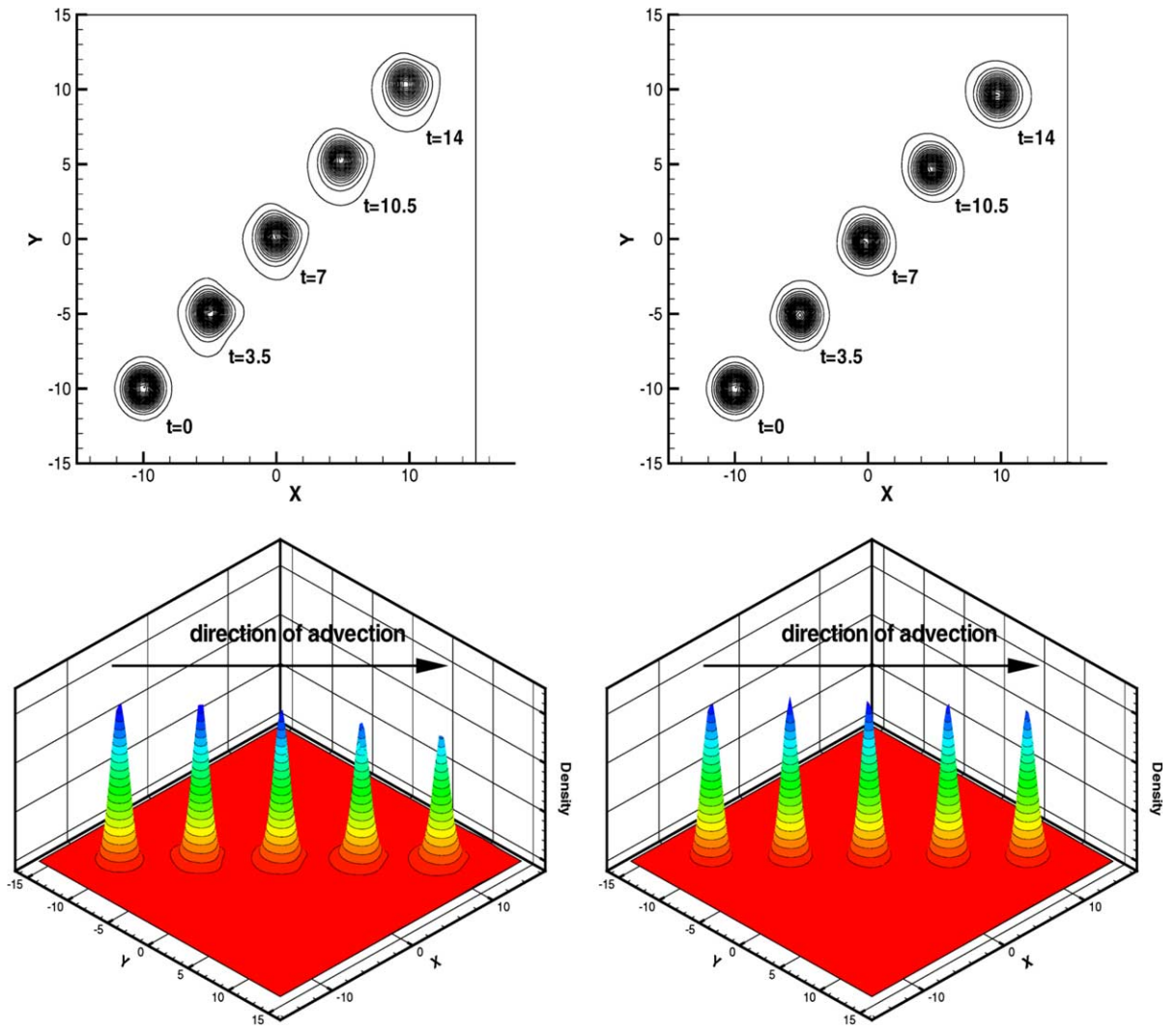

Fig. 1. Advection of a vortex. Isovalues of density on a 100×100 grid during the vortex advection along the grid diagonal. Left: DNC scheme. Right: RBC scheme.

4.2. Vortex pairing in a time-developing mixing layer

An initial x-velocity distribution is defined as follows:

$$u = 0.5\tanh(2y)$$

while the y-velocity v is everywhere equal to 0. The velocities in the upper flow when $y \to +\infty$ will be denoted u_1 while the velocity in the lower flow when $y \to -\infty$ will be denoted u_2. The velocity are normalized by the velocity jump across the shear layer $(u_1 - u_2)$ and the reference length is the vorticity thickness δ_ω defined by

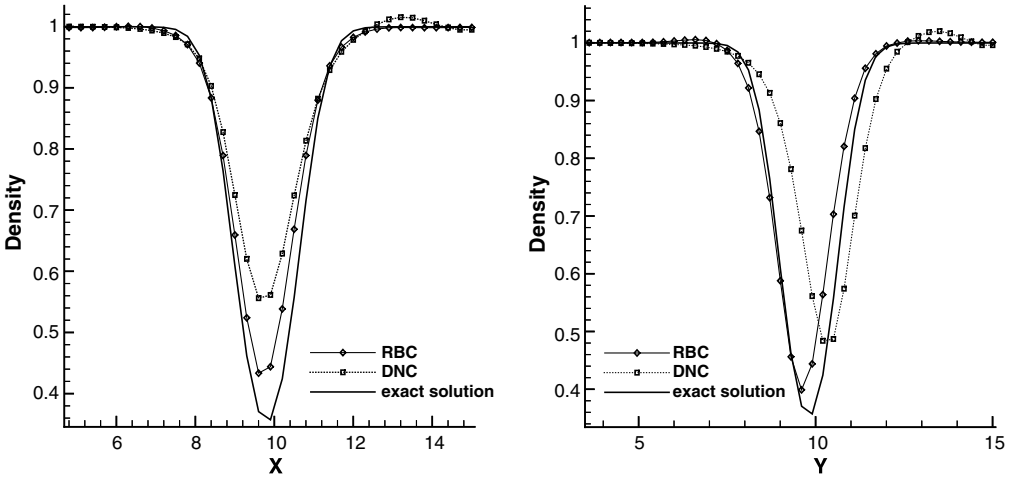

Fig. 2. Advection of a vortex. Density profiles at time $t = 14$ along an horizontal (left) and a vertical (right) line passing through the exact location of the vortex core.

$$\delta_\omega = \frac{u_1 - u_2}{(\mathrm{d}u/\mathrm{d}y)_{\max}}$$

The stagnation enthalpy is assumed to be constant. Since $u_2 = -u_1$, this means both fluid streams have the same sound velocity and therefore temperature when $y \to \pm\infty$. This sound velocity $c_1 = c_2$ is deduced from the value of the convective Mach number $M_c = \frac{u_1 - u_2}{c_1 + c_2}$ fixed at 0.8. The pressure is assumed to be uniform through the mixing layer so that the upper and lower flows have also the same density when $y \to \pm\infty$. The density is computed from the constant stagnation enthalpy assumption and is given by

$$\rho = \rho_1 \Big/ \left(1 + \frac{\gamma - 1}{2}\,\frac{u_1^2 - u^2}{c_1^2}\right)$$

The Reynolds number based on the velocity jump, the vorticity thickness and the kinematic viscosity at the freestream temperature is set equal to 1000; the Prandtl number is equal to 0.72. The instability of this mixing layer is then initiated by adding disturbances to the velocity components which correspond approximately to eigenfunctions of the linear stability problem for such a compressible mixing layer. All the details of the test case set-up are those given in [14], which will allow a comparison between the present computations and the numerical results presented in this previous work. The y-component of the initial velocity field is perturbed by

$$v' = \sum_{k=1}^{2} a_k \cos\left(\frac{2\pi k x}{L_x} + \phi_k\right) \exp\left(-\frac{y^2}{b}\right)$$

where L_x is the box-length in the x-direction and the y-modulation b is set to 10. Vortex pairing in the center of the computational domain is obtained by choosing the initially most unstable wave $k = 2$ to have amplitude $a_2 = 0.05$ and phase $\phi_2 = -\pi/2$ and the subharmonic wave $k = 1$ with $a_1 = 0.01$ and $\phi_1 = -\pi/2$. The perturbation on the x-component of velocity is obtained by

assuming the total perturbation is divergence free. The computational domain extends from $y = -L_y/2$ up to $y = L_y/2$ with $L_y = 100$ and from $x = 0$ up to $x = L_x$ with $L_x = 30$. The grid is uniform in the x-direction and stretched in the y-direction to ensure a good representation of the mixing layer, using the mapping:

$$y = \frac{L_y}{2}\frac{\sinh(b_y\eta)}{\sinh(b_y)}$$

with a coordinate η equally spaced on $[-1, +1]$ and a stretching factor $b_y = 3.4$. Periodic boundary conditions are applied at $x = 0$ and $x = L_x$ while lower and upper boundaries are treated as slip walls. The time evolution of the flow is computed up to $t = 160$. Following other authors [8,14,21] we choose to analyze the temperature distribution. The time-evolution of the temperature contours computed by RBC and DNC on a 201×201 grid with a physical time-step $\Delta t = 0.1$ is plotted on Fig. 3 along with the results obtained in [14] on the same grid and for the same time-step using a fourth-order central scheme with second-order upwind TVD dissipation and non-linear characteristic filters to control the amount of this added dissipation as well as a classical fourth-order Runge–Kutta discretization for time integration. The methods RBC and DNC, which share a similar second-order three-level implicit discretization of the physical time-derivative, yield very close results on such a fine grid, which compare also very well with those of Yee et al. A more detailed comparison of RBC and DNC is performed with a larger time-step ($\Delta t = 0.5$), allowed by the implicitation with respect to the dual time, on a series of increasingly coarsened grids (see Fig. 4) containing respectively 181×181, 121×121 and 61×61 points. Here again, the solutions on the finest grid are very similar; however RBC provides better shock resolution (almost oscillation-free) and is less sensitive to grid coarsening with, in particular, better preserved vortex structures on the coarsest grid. This lesser sensitivity of the RBC approach to grid coarsening is also made clear on the cutlines plotted in Fig. 5.

4.3. Shock wave impingement on a spatially evolving mixing layer

The computational domain is a rectangular box extending from $x = 0$ up to $x = 200$ and from $y = -20$ up to $y = +20$. A hyperbolic tangent profile $u = 2.5 + 0.5\tanh(2y)$ is specified along the inflow boundary $x = 0$. Equal pressures and stagnation enthalpies are assumed for the lower and upper flows. The convective Mach number is set equal to 0.6. The reference density is chosen as the average of the two free streams and the reference pressure as $(\rho_1 + \rho_2)(u_1 - u_2)^2/2$. This allows to compute the values of the upper and lower states on the inflow boundary (see [14] for more details). The Reynolds number is chosen to be 500 and the Prandtl number is still 0.72. The following fluctuations are added to the y-component of the inflow velocity only:

$$v' = \sum_{k=1}^{2} a_k \cos\left(\frac{2\pi k t}{T} + \phi_k\right)\exp\left(-\frac{y^2}{b}\right)$$

where the period T is given by $T = \lambda/u_c$ with a wavelength $\lambda = 30$ and a convective velocity $u_c = (u_1c_2 + u_2c_1)/(c_1 + c_2)$. The y-modulation is kept equal to 10 and $(a_k, \phi_k) = (0.05, 0)$ for $k = 1$ and $(0.05, \pi/2)$ for $k = 2$.

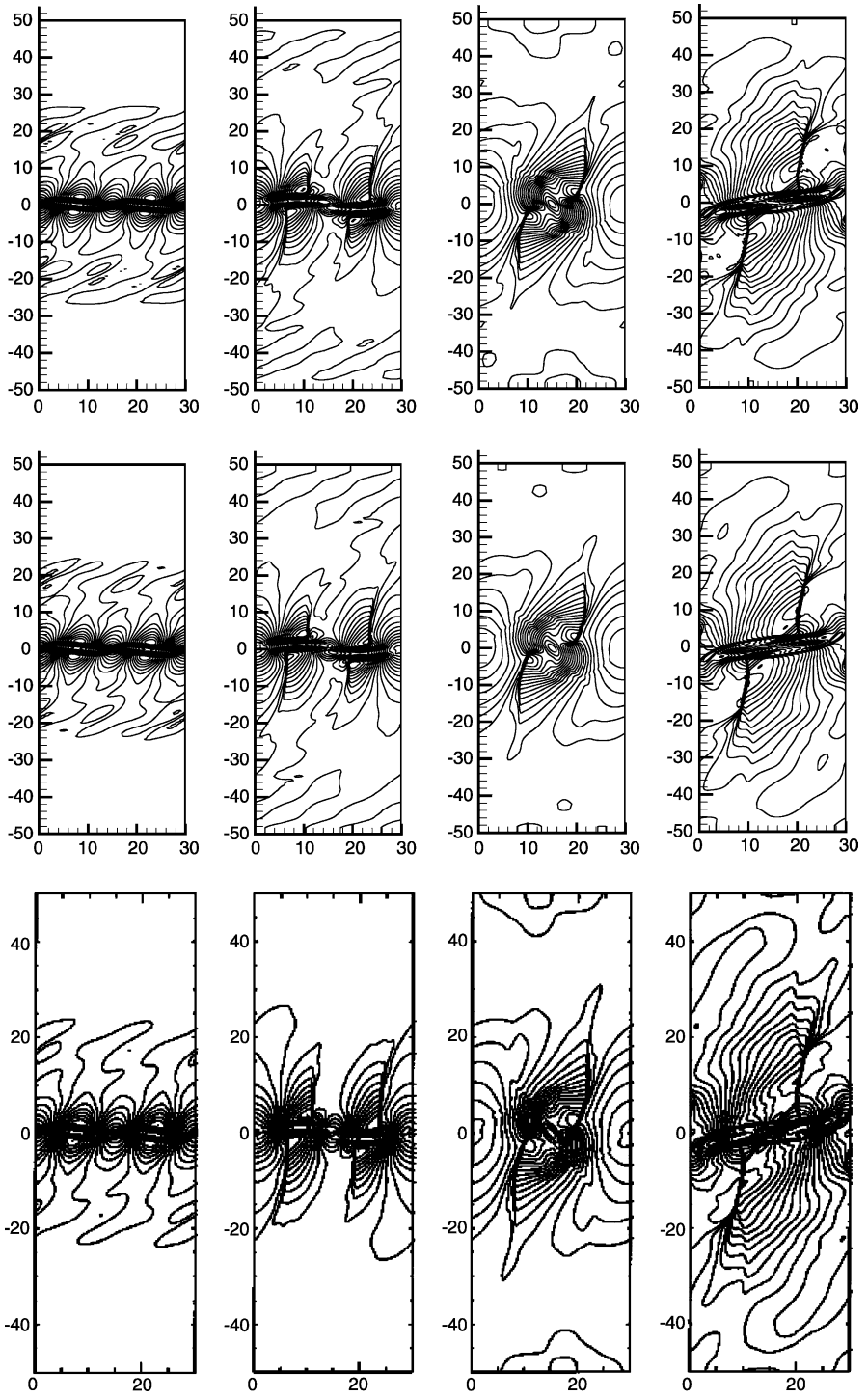

Fig. 3. Vortex pairing. Contours of temperature at time $t = 40$, 80, 120 and 160 (from left to right) on a 201×201 grid with $\Delta t = 0.1$. Top: RBC results. Middle: DNC results. Bottom: reference results obtained in [14].

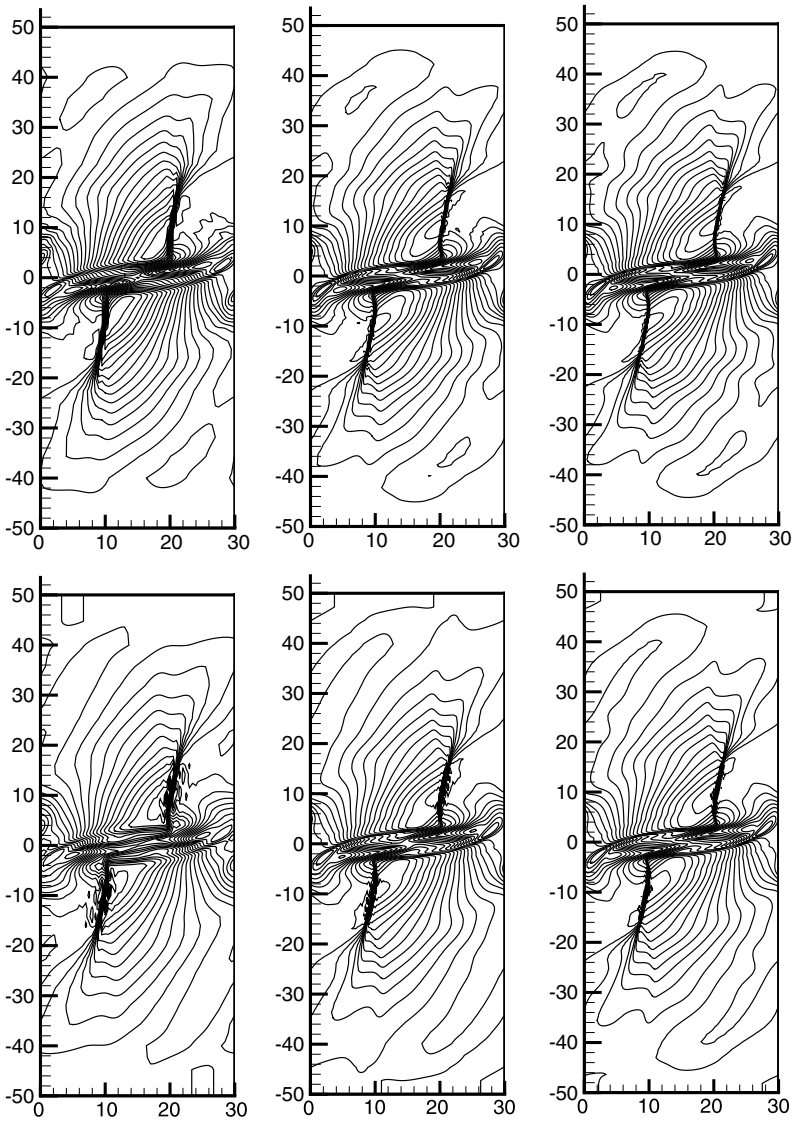

Fig. 4. Vortex pairing. Temperature contours at $t = 160$. Grid-convergence for the RBC (top) and DNC (bottom) schemes.

The state along the upper boundary is chosen so as to generate an oblique shock with angle $\beta = 12^\circ$ from the top left-hand corner of the domain; this shock impacts on the spatially evolving shear layer which is deflected by the interaction. The shock wave below the shear layer reflects on the lower boundary treated as a slip wall and crosses back the unstable shear layer. The flow leaves the computational domain with supersonic speed along the whole outflow boundary which allows a simple extrapolation of the variables on this boundary from the neighbouring interior values. The solutions computed on a 401×101 grid using RBC and DNC are compared with those

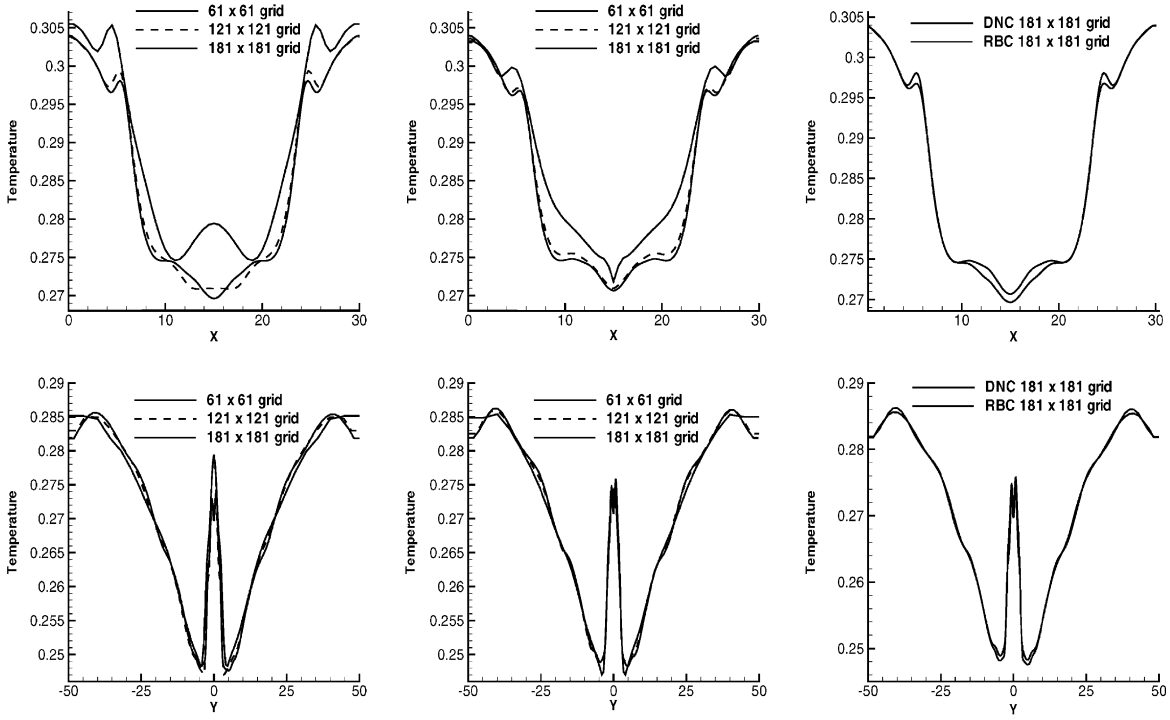

Fig. 5. Vortex pairing. The cutlines of temperature along the horizontal centerline $y = 0$ (top) and the vertical centerline $x = 15$ (bottom) are plotted for three levels of grid refinement. From left to right: DNC results, RBC results and DNC/RBC on the fine grid.

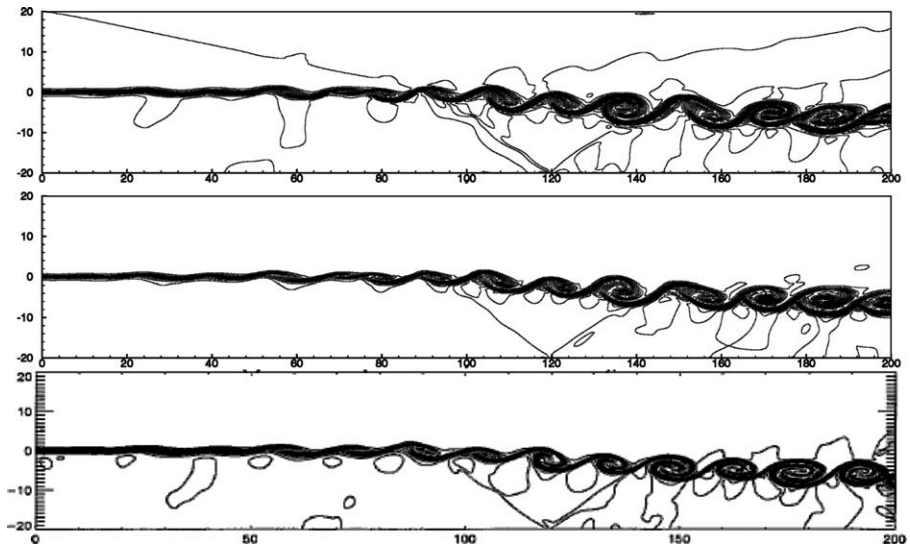

Fig. 6. Shock–shear-layer interaction. Contours of temperature at time $t = 120$. Top: DNC results on a 401×101 grid. Middle: RBC results on the same grid. Bottom: reference results [14] on a 641×161 grid.

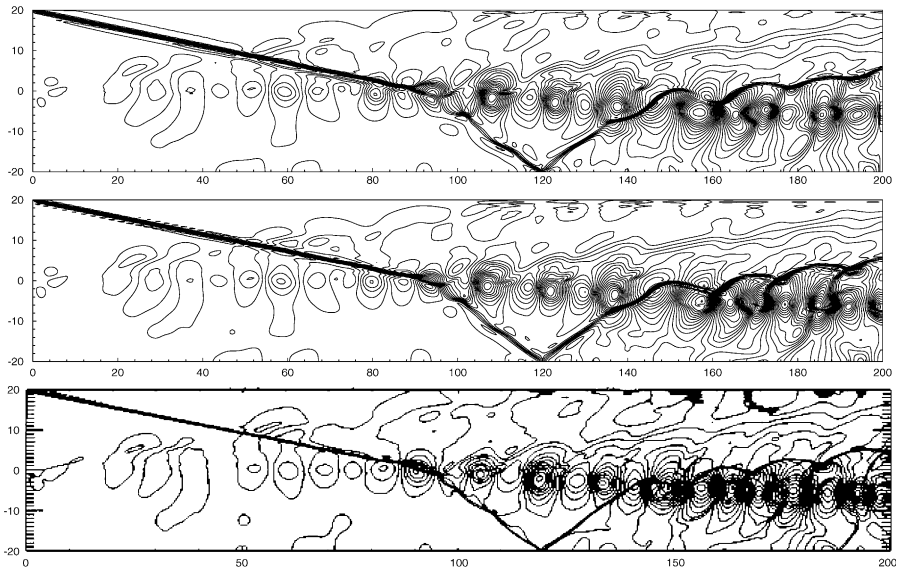

Fig. 7. Shock–shear-layer interaction. Contours of pressure at time $t = 120$. Top: DNC results on a 401×101 grid. Middle: RBC results on the same grid. Bottom: reference results [14] on a 641×161 grid.

of [14] given again by a fourth-order central scheme with second-order upwind TVD dissipation and non-linear characteristic filters along with a classical fourth-order Runge–Kutta time-discretization, applied on a finer 641×161 grid. The contours of temperature and pressure for the three methods are displayed respectively on Figs. 6 and 7. The DNC and RBC results compare rather well with those of [14] in the sense that the global flow features are correctly captured. However discrepancies are observed in particular on the pressure contours in the region where the reflected shock crosses back the destabilized shear layer and downstream of this interaction; these may be due to the lower order of time integration used in the DNC and RBC calculation. Nonetheless the present problem demonstrates the ability of the RBC scheme to handle the computation of complex unsteady flows involving shocks.

5. Conclusion

This paper has presented a residual-based scheme for computing unsteady solutions of the compressible Euler and Navier–Stokes equations. It makes use of the residual $r = w_t + f_x + g_y$ vanishing at steady state with respect to a dual time τ to build a compact dissipation-like operator, of order 1 in the transient phase but which becomes third-order accurate when $w_\tau \to 0$. Similarly, third-order accuracy in space is obtained by correcting the simply centered fluxes so as to yield a global truncation error with second-order terms depending only on derivatives of r and therefore vanishing at steady state. The physical time-derivative is systematically discretized at second order using a three-level implicit formula. This residual-based scheme has been compared with a conventional upwind scheme approximating separately at third order the inviscid fluxes and using the same second-order implicit time-integration. The computation of the simple advection of a vortex

has shown the reduced dissipative and dispersive error of the RBC approach. Complex flows involving shocks have also been accurately computed using the RBC approach, even on coarse grids, demonstrating the robustness of the method without limiters or other corrections.

The RBC scheme has already been successfully and easily extended to the computation of 3D steady flows [12]; the application of the present unsteady method to 3D problems should therefore be immediate. Previous developments have also been devoted to the formulation of the RBC scheme on non-uniform [22] and fully irregular [23] grids. Our near future research will focus on the extension of these formulations to the unsteady case, using the approach we have detailed here, with a view at computing unsteady flows of interest for the aeronautics industry, such as the low-frequency self-induced shock oscillations typical of transonic buffet.

References

[1] Hirsh RS. High order accurate difference solutions of fluid mechanics problems by a compact differencing technique. J Comput Phys 1975;19:90–109.
[2] Peyret R. A Hermitian finite-difference method for the solution of the Navier–Stokes equations. In: Proc 1st Intern Conf on Numerical Methods in Laminar and Turbulent Flows. Pentech Press; 1978. p. 45–54.
[3] Abarbanel S, Kumar A. Compact high-order schemes for the Euler equations. J Sci Comput 1988;3:275–88.
[4] Lele SK. Compact finite difference schemes with spectral-like resolution. J Comput Phys 1992;103:16–42.
[5] Cockburn B, Shu CW. Nonlinearly stable compact schemes for shock calculations. SIAM J Numer Anal 1994;31:607–27.
[6] Tolstykh AI. High accuracy non-centered compact difference schemes for fluid dynamics applications. Singapore: World Scientific; 1994.
[7] Lerat A, Rezgui A. Schémas dissipatifs précis à l'ordre trois pour les systèmes hyperboliques. CR Acad Sci Paris 1996;323(II b):397–403.
[8] Fu D, Ma Y. A high order accurate difference scheme for complex flow fields. J Comput Phys 1997;134:1–15.
[9] Yee HC. Explicit and implicit multidimensional compact high-accurate resolution shock-capturing methods: formulation. J Comput Phys 1997;131:216–32.
[10] Visbal MR, Gaitonde DV. High-order-accurate methods for complex unsteady subsonic flows. AIAA J 1999;37:1231–9.
[11] Abgrall R, Mezine M. A compact residual scheme for unsteady compressible flow problems. In: Armfield S, Morgan P, Srinivas, editors. Computational Fluid Dynamics 2002. Berlin: Springer; 2003. p. 165–70.
[12] Lerat A, Corre C. Residual-based compact schemes for multidimensional hyperbolic system of conservation laws. Comput Fluids 2002;31:639–61.
[13] Lerat A, Corre C. A residual-based compact scheme for the compressible Navier–Stokes equations. J Comput Phys 2001;170:642–75.
[14] Yee HC, Vinokur M, Djomehri MJ. Entropy splitting and numerical dissipation. J Comput Phys 2000;162:33–81.
[15] Peyret R, Taylor T. Computational methods for fluid flows. New York: Springer; 1983.
[16] Jameson A. Time-dependent calculations using multigrid with applications to unsteady flows past airfoils and wings. AIAA Paper 1991:91–1596.
[17] Lerat A, Sidès J. Efficient solution of the steady Euler equations with a centered implicit method. In: Morton KW, Baines MJ, editors. Numerical methods for fluid dynamics, vol. 3. Oxford: Clarendon Press; 1988. p. 65–86.
[18] Lerat A. Multidimensional centred schemes of the Lax–Wendroff type. In: Hafez M, Oshima K, editors. CFD Review 1995. John Wiley; 1995. p. 124–40.
[19] Corre C, Khalfallah K, Lerat A. Line-relaxation methods for a class of centred schemes. Comput Fluid Dynam J 1996;5:213–46.
[20] Rezgui A, Cinnella P, Lerat A. Third-order accurate finite volume schemes for Euler computations on curvilinear meshes. Comput Fluids 2001;30:875–901.

[21] Lumpp T. Compressible mixing layer computations with high-order ENO schemes. In: 15th Intl Conf on Num Meth in Fluid Dynamics, Monterey, USA, June 1996. Lecture Notes in Physics 1997;490:99–104.
[22] Lerat A, Corre C, Hanss G. Efficient high-order schemes on non-uniform meshes for multi-D compressible flows. In: Caughey DA, Hafez M, editors. Frontiers of computational fluid dynamics–2002. Singapore: World Scientific; 2002. p. 89.
[23] Hanss G, Corre C, Lerat A. High-order schemes on irregular structured meshes for multi-dimensional compressible flows. In: ECCOMAS CFD 2001, Swansea, UK, CD Rom Proceed, 2001.